INSTITUTE OF PHYSICS PUBLISHING JOURNAL OF PHYSICS: CONDENSED MATTER

J. Phys.: Condens. Matter **17** (2005) 6285–6300 doi:10.1088/0953-8984/17/39/013

High pressure effects on the structural and vibrational properties of antiferromagnetic $KFe(MoO_4)_2$

M Mączka[1], A Pietraszko[1], G D Saraiva[2], A G Souza Filho[2], W Paraguassu[2], V Lemos[2], C A Perottoni[3,4], M R Gallas[4], P T C Freire[2], P E Tomaszewski[1], F E A Melo[2], J Mendes Filho[2] and J Hanuza[1,5]

[1] Institute of Low Temperature and Structure Research, Polish Academy of Sciences, PO Box 1410, 50-950 Wrocław 2, Poland
[2] Universidade Federal do Ceará, Departamento de Física, PO Box 6030, CEP 60455-900, Fortaleza, CE, Brazil
[3] Universidade de Caxias do Sul, Centro de Ciências Exatas e Tecnologia, Departamento de Física e Química, 95070-560 Caxias do Sul, RS, Brazil
[4] Universidade Federal do Rio Grande do Sul, Instituto de Física, Laboratório de Altas Pressões e Materiais Avançados, 91501-970 Porto Alegre, RS, Brazil
[5] Department of Bioorganic Chemistry, Faculty of Industry and Economics, Wrocław University of Economics, 118/120 Komandorska Street, 53-345 Wrocław, Poland

Received 21 June 2005, in final form 9 August 2005
Published 16 September 2005
Online at stacks.iop.org/JPhysCM/17/6285

Abstract

The crystal structure of the paraelastic phase of $KFe(MoO_4)_2$ at 360 K was reinvestigated and high pressure Raman scattering experiments were performed on this material. The studies indicated that this molybdate crystallizes in the $P\bar{3}m1$ structure above 312 K. At room temperature the structure is monoclinic and it transforms under pressure into $P\bar{3}m1$, $P\bar{3}c1$ and low symmetry phases at 0.25, 1.3 and 1.6 GPa, respectively. The phase transitions observed at 0.25 and 1.6 GPa are irreversible whereas the 1.3 GPa transition is reversible. The lattice dynamics calculations performed for the $P\bar{3}m1$ phase allowed us to obtain an assignment of observed modes and helped us to obtain insight into the mechanism driving the structural changes occurring in this material. The x-ray study of the highest pressure phase, recovered during the decompression experiment, shows that the crystal structure of this phase is monoclinic or triclinic. When this phase is subjected to heat treatment at 673 K, it either transforms into another phase or decomposes.

1. Introduction

$KFe(MoO_4)_2$ belongs to the family of layered trigonal molybdates and tungstates with chemical formula $M^+M^{3+}(MoO_4)_2$, where M^+ = Na, K, Rb, Cs and M^{3+} = Al, Sc, Cr, Fe [1–4]. These materials have been the subject of many studies owing to the richness of structural instabilities induced either by heat or hydrostatic pressure [1–6]. Recently, $KFe(MoO_4)_2$ and

$RbFe(MoO_4)_2$ molybdates attracted considerable attention since these compounds constitute rare examples of nearly two-dimensional 'triangular' antiferromagnets available in single-crystal form [7–9].

The aim of the present work is to gain information on the structural changes occurring in $KFe(MoO_4)_2$ crystal under hydrostatic pressure and the pressure dependence of the phonon properties. The Raman technique was employed for this purpose because it proved to be a valuable tool in molybdate and tungstate phase transition investigations in the past [1–6]. Therefore, $KFe(MoO_4)_2$ Raman scattering may help us to understand the driving mechanism of structural changes observed in this crystal and other related layered materials. For a better understanding of such mechanisms, detailed information on the crystal structure of the prototype phase is required.

In previous published works the trigonal phase of this family of crystals is described as belonging to either the $P\bar{3}m1 = D^3_{3d}$ space group with $a \sim 5$–6 Å and $c \sim 7$–8 Å or the $P\bar{3}c1 = D^4_{3d}$ space group with $a \sim 5$–6 Å and $c \sim 14$–15 Å [10–12]. The room temperature x-ray diffraction studies of $KFe(MoO_4)_2$ show that the c unit cell parameter is 14.24 Å and its crystal structure was obtained by Klevtsova *et al* by assuming the $P\bar{3}c1$ structure, accordingly [10]. However, later optical studies revealed that this crystal exhibits two ferroelastic phase transitions at $T_1 = 312$ K and $T_2 = 139$ K into monoclinic and triclinic phases, respectively [1, 13]. On the basis of this finding, the room temperature phase should be monoclinic and the remaining data on the crystal structure of $KFe(MoO_4)_2$ in the literature may be incorrect. This controversy requires further investigation of the crystal structure of $KFe(MoO_4)_2$, particularly in the case of the prototype phase, for temperatures above the ferroelastic phase transition reported as 312 K.

In this paper we reinvestigate this prototype phase by performing x-ray diffraction measurements at 360 K, well above the T_1 phase transition temperature. The analysis of our data shows that the crystal structure of the prototype phase is not $P\bar{3}c1$, as previously assumed, but $P\bar{3}m1$. Using $P\bar{3}m1$ as the space group of the prototype phase we performed lattice dynamics calculations of Brillouin zone centre phonon modes to obtain the eigenvalues and their corresponding eigenmodes. The results were employed to assign the bands in the Raman spectrum of the prototype phase of $KFe(MoO_4)_2$. We also investigated the pressure dependence of $KFe(MoO_4)_2$ Raman spectra which revealed a rich sequence of phase transitions in the 0.0–4.0 GPa pressure range.

2. Experiment

2.1. Sample preparation

The $KFe(MoO_4)_2$ crystals were grown from the flux. The mixture of K_2CO_3, Fe_2O_3 and MoO_3, corresponding to the compositions $KFe(MoO_4)_2$ and $K_2Mo_2O_7$ in a ratio 1:1, was placed in a platinum crucible, heated to 800 °C, kept at this temperature for 40 h, cooled at a rate of 2 °C h^{-1} to 600 °C and then cooled at a rate 10 °C h^{-1} to room temperature. The light green crystals of optical quality obtained were extracted from the crucible by washing with hot water.

2.2. Ambient pressure x-ray experiments and structure refinement

The x-ray diffraction data on $KFe(MoO_4)_2$ single crystal at ambient pressure were collected using an automatic x-ray four-circle KUMA Diffraction diffractometer with CCD area detectors. Graphite monochromated Mo Kα radiation ($\lambda = 0.071\,073$ nm) was generated at 50 kV and 23 mA. A single image for 1° rotation around the ω axis was obtained in 30 s and the full set of x-ray diffraction data in the 2θ angle was collected over the range from 3°

Table 1. Crystal data and structure refinement for $KFe(MoO_4)_2$ at 360 K.

Empirical formula	$KFe(MoO_4)_2$
Formula weight	414.83
Temperature	360(2) K
Wavelength	0.71073 Å
Crystal system, space group	Trigonal, $P\bar{3}m1$
Unit cell dimensions	$a = 5.6650(8)$ Å $\alpha = 90°$
	$b = 5.6650(8)$ Å $\beta = 90°$
	$c = 7.1380(14)$ Å $\gamma = 120°$
Volume	198.38(6) $Å^3$
Z, calculated density (Mg m^{-3})	1, 3.472
Absorption coefficient	5.467 mm^{-1}
$F(000)$	193
Crystal size	$0.24 \times 0.18 \times 0.14$ mm^3
Theta range for data collection	5.05°–46.29°
Index ranges	$-11 \leqslant h \leqslant 5, -10 \leqslant k \leqslant 11, -9 \leqslant l \leqslant 14$
Reflections collected/unique	3599/666 (R(int) = 0.0280)
Completeness to $2\Theta = 46.29$	94.2%
Refinement method	Full-matrix least squares on F^2
Data/restraints/parameters	666/0/18
Goodness-of-fit on F^2	1.020
Final R indices ($I > 2\sigma(I)$)	$R_1 = 0.0229$, $wR_2 = 0.0420$
R indices (all data)	$R_1 = 0.0273$, $wR_2 = 0.0429$
Extinction coefficient	0.094(3)
Largest diff. peak and hole	1.442 and −1.743 e $Å^{-3}$

to 93°. The intensities of the reflections were recorded in 1200 frames (each frame consisting of 512 × 512 pixels with 2 × 2 pixel binning). The lattice parameters were calculated for refinement of positions of all measured reflections. The measurements were performed at 360 K with a KUMA Diffraction temperature stage, the temperature of which was stabilized to within 0.5 K. The analytical absorption correction for all samples was calculated with the CrysAlis procedure [14]. Details of data collection and structure refinement are presented in table 1. The crystal structure at 360 K was obtained using the direct method—with the SHELXL-97 program [15]. The same program was used for the successive cycles of refinement of the crystal structure.

2.3. In situ high pressure Raman experiments

The pressure dependent Raman spectra were obtained with a Jobin-Yvon T64000 spectrometer operating in the double-subtractive mode, equipped with a N_2-cooled charge coupled device (CCD) detection system. The 514.5 nm line of an argon ion laser was used as the excitation. An Olympus microscope lens with a focal distance $f = 20.5$ mm and numeric aperture NA = 0.35 was used to focus the laser beam on the sample surface. High pressure Raman experiments were performed at room temperature using a diamond anvil cell (DAC) with 4:1 methanol:ethanol mixture as the transmitting fluid. The pressure calibration was achieved by using the well known pressure shift of the ruby luminescence lines. The spectrometer slits were set for a resolution of 2 cm^{-1}.

2.4. Ex situ high pressure x-ray experiments

The high pressure/high temperature x-ray experiments were carried out using a toroidal-type chamber (a detailed description of this high pressure method is given elsewhere [16, 17]). The

Table 2. Atomic coordinates ($\times 10^4$) and equivalent isotropic displacement parameters ($Å^2 \times 10^3$) for $KFe(MoO_4)_2$ at 360 K. U(eq) is defined as one third of the trace of the orthogonalized U_{ij} tensor.

	x	y	z	U(eq)
Fe(1)	0	0	5000	12(1)
Mo(1)	6667	3333	2582(1)	12(1)
K(1)	0	0	0	38(1)
O(1)	8381(1)	6762(2)	3335(2)	34(1)
O(2)	6667	3333	179(3)	31(1)

temperature was measured with a chromel–alumel type K thermocouple encapsulated in an Al_2O_3 sleeve. The pressure cell consisted of a graphite heater (height of 9.2 mm, diameter of 7.0 mm, wall thickness of 1.5 mm), two small discs of fired pyrophyllite and two h-BN discs (diameter of 4.0 mm). A capsule of h-BN (3.0 mm internal diameter) is placed between these discs, and inside it, the sample. In this experimental set-up, h-BN acts as a nearly hydrostatic pressure-transmitting medium and, in lower temperature experiments (up to 800 °C), it behaves as an inert material. The pressure calibration was performed by the 'fixed points' technique [16]. Two metals were used, Bi and Yb, which allowed calibrating the pressure using the following three fixed points: Bi with phase transitions at 2.5 and 7.7 GPa, and Yb with a phase transition at 4.0 GPa. The pressure is considered accurate to ±0.5 GPa. In a typical experiment, the samples were compacted at 4.0 GPa at room temperature. A small piece of Yb was put on top of the sample in order to check the applied pressure. After pressure stabilization, the sample was maintained at this pressure for 15 min. In the high temperature experiment, the sample processed at high pressure was subjected to heat treatment up to 653 K, under an argon atmosphere, kept in this temperature for 30 min, cooled down, and heated again to the same temperature for 150 min. In the high temperature, high pressure experiment, after pressure stabilization at 4.0 GPa, the sample (without the Yb gauge) was heated to 673 K for 30 min. Quenching was processed by turning off the power and, after 5–10 min, pressure was released.

X-ray diffraction data on the pristine and quenched samples were obtained at ambient conditions with a Siemens D500 diffractrometer equipped with Soller slits in the incident beam, a 1° divergence slit, a 0.15 mm receiving slit, and a graphite monochromator in the secondary beam. Data were collected with Cu Kα radiation, in the angular range from 5° to 100° (2θ°), with a scan step of 0.05° and an acquisition time of 1.0 s per step for the pristine sample, 2.0 s per step for the samples processed at high pressure and room temperature, and 4.0 s for the sample processed at high pressure and high temperatures.

3. Results and discussion

3.1. X-ray diffraction studies at 360 K

X-ray diffraction results show that $KFe(MoO_4)_2$ crystallizes, at 360 K, in the centrosymmetric space group $P\bar{3}m1$ with lattice parameters that are given in table 1. This result shows that the previously assumed $P\bar{3}c1$ symmetry [10] is not correct and $KFe(MoO_4)_2$ crystallizes in the same space group, $P\bar{3}m1$, as the majority of trigonal double molybdates and tungstates. Final parameters together with the equivalent thermal displacement amplitudes U_{eq} and anisotropic displacement parameters are listed in tables 2 and 3. Supplementary data for this structure are available in CIF format from the authors.

The crystal structure consists of MoO_4 tetrahedra bound to the FeO_6 octahedra through O(2) oxygen atoms as shown in figure 1. The bound MoO_4 tetrahedra and FeO_6 octahedra

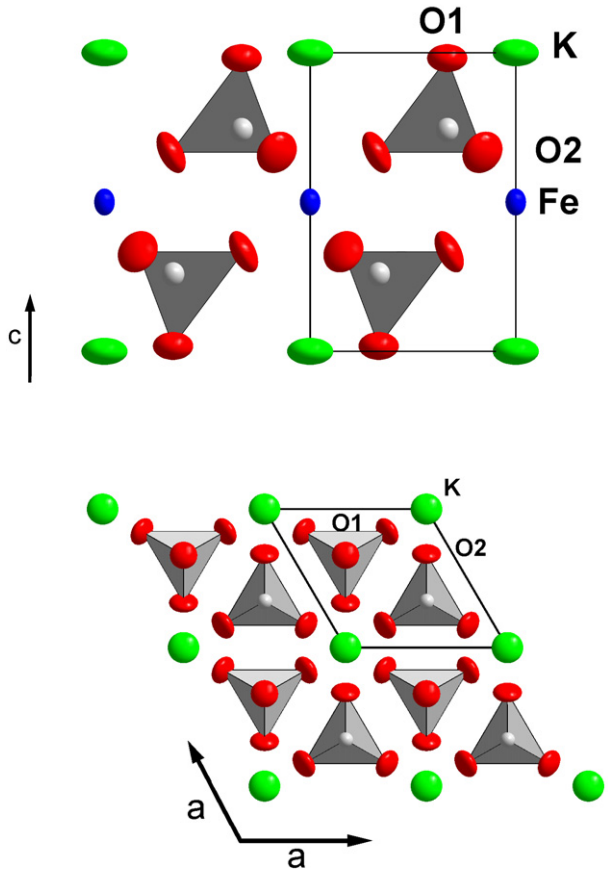

Figure 1. View of the $P\bar{3}m1$ crystal structure of $KFe(MoO_4)_2$ along with the a axis (upper part) and c axis (lower part). The Mo atoms are placed in the centres of the tetrahedra shown.
(This figure is in colour only in the electronic version)

Table 3. Anisotropic displacement parameters ($Å^2 \times 10^3$) for $KFe(MoO_4)_2$ at 360 K. The anisotropic displacement factor exponent takes the form $-2\pi i^2[h^2a^{*2}U_{11} + \cdots + 2hka^*b^*U_{12}]$.

	U_{11}	U_{22}	U_{33}	U_{23}	U_{13}	U_{12}
Fe(1)	10(1)	10(1)	17(1)	0	0	5(1)
Mo(1)	12(1)	12(1)	13(1)	0	0	6(1)
K(1)	49(1)	49(1)	17(1)	0	0	24(1)
O(1)	37(1)	20(1)	39(1)	−14(1)	−7(1)	10(1)
O(2)	37(1)	37(1)	18(1)	0	0	19(1)

form layers perpendicular to the c axis. K atoms form layers of a second type perpendicular to the c axis. These ions are surrounded by 12 oxygen atoms forming a distorted cubic cubo-octahedron. The distances between potassium and oxygen atoms are 2.856(3) Å and 3.270(3) Å for O(1) and O(2), respectively. It is worth noting that the two non-equivalent oxygen atoms in the MoO_4 tetrahedra are involved in different interactions, i.e., whereas the

Table 4. The correlation diagram showing the correspondence between the optical modes in the $P\bar{3}m1$ and $P\bar{3}c1$ structures of $KFe(MoO_4)_2$ (the data for the $P\bar{3}c1$ structure are given in parentheses).

Ion	Free ion symmetry	Site symmetry	Factor group symmetry
MoO_4^{2-}	T_d	$C_{3v}(C_3)$	$D_{3d}(D_{3d})$
	$\nu_1 - A_1$	$A_1(A)$	$A_{1g}(A_{1g} + A_{2g})$
			$A_{2u}(A_{1u} + A_{2u})$
	$\nu_2 - E$	E(E)	$E_g(2E_g)$
			$E_u(2E_u)$
	ν_3, ν_4, translation $- F_2$	$A_1(A)$	A_{1g} $(A_{1g} + A_{2g})$
			$A_{2u}(A_{1u} + A_{2u})$
		E(E)	$E_g(2E_g)$
			$E_u(2E_u)$
	Libration $- F_1$	$A_2(A)$	$A_{2g}(A_{1g} + A_{2g})$
			$A_{1u}(A_{1u} + A_{2u})$
		E(E)	$E_g(2E_g)$
			$E_u(2E_u)$
K^+		$D_{3d}(D_3)$	$D_{3d}(D_{3d})$
		$A_{2u}(A_2)$	$A_{2u}(A_{2u} + A_{2g})$
		$E_u(E)$	$E_u(E_u + E_g)$
Fe^{3+}		$D_{3d}(C_{3i})$	$D_{3d}(D_{3d})$
		$A_{2u}(A_u)$	$A_{2u}(A_{1u} + A_{2u})$
		$E_u(E_u)$	$E_u(2E_u)$

O(2) atoms are relatively strongly bound to Fe atoms, the O(1) atoms interact weakly and only with potassium atoms.

3.2. Lattice dynamics

First the symmetry and vibrational properties of the $P\bar{3}m1$ structure of $KFe(MoO_4)_2$ will be described in order to establish a basis for discussing the high pressure Raman results. For this trigonal structure, group theory predicts nine Raman active modes which are [7]

$$\Gamma_{\text{Raman}} = 4A_{1g} + 5E_g.$$

These Raman modes can be subdivided into symmetric stretching ($\nu_1 - A_{1g}$), asymmetric stretching ($\nu_3 - A_{1g} + E_g$), symmetric bending ($\nu_2 - E_g$), asymmetric bending ($\nu_4 - A_{1g} + E_g$), translational ($A_{1g} + E_g$), and librational (E_g) modes of the MoO_4^{2-} ions (see the correlation diagram presented in table 4). The Raman spectra of $KFe(MoO_4)_2$ crystal measured at room temperature are shown figures 2 and 3.

In order to adequately assign the Raman peaks to the atomic vibrations, we performed lattice dynamics calculations giving as results both frequencies (eigenvalues) and atomic displacements (eigenvectors) for each Raman active normal mode. Since $KFe(MoO_4)_2$ is mostly ionic, we performed the calculations on the basis of a partially ionic model described in the paper by Nozaki *et al* [18]. The atomic positions used in the calculations were taken from our present x-ray data. The following interatomic potential was used in the lattice dynamics calculations:

$$U_{ij}(r_{ij}) = \frac{z_i z_j e^2}{r_{ij}} + (b_i + b_j)\exp\left[\frac{a_i + a_j - r_{ij}}{b_i + b_j}\right] - \frac{c_i c_j}{r_{ij}^6} + D_{ij}(\exp[-2\beta_{ij}(r_{ij} - r_{ij}^*)] - 2\exp[-2\beta_{ij}(r_{ij} - r_{ij}^*)]).$$

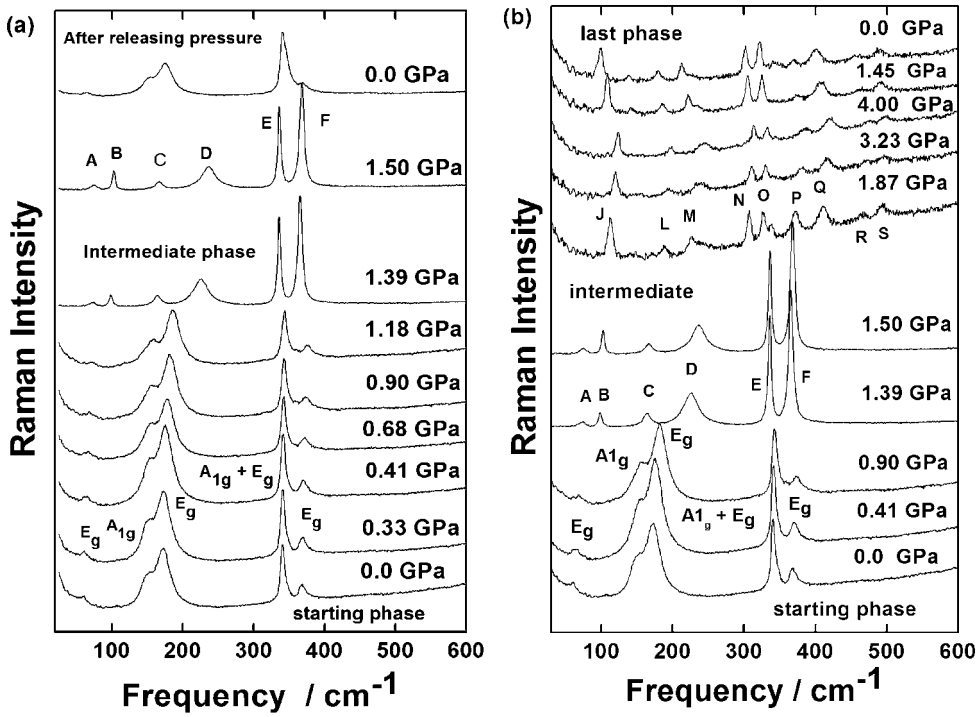

Figure 2. (a) Raman spectra of $KFe(MoO_4)_2$ crystal in the low frequency region recorded at different pressures during compression and decompression experiments performed in the 0–1.5 GPa pressure range. (b) The same as in (a) except that the data are for the 0–4.0 GPa pressure range.

This interatomic potential consists of: a Coulomb interaction (first term) to model the long range interactions; a Born–Mayer-type repulsive interaction (second term) for accounting the short range forces; a van der Waals attractive interaction (third term) to model the dipole–dipole interaction; and, finally, the Morse potential contribution (last term) to take into account the covalent bond character. z_i and z_j are the effective charges of the ions i and j, respectively, separated by the distance r_{ij}. The parameters (a_i, a_j) and (b_i, b_j) correspond to the ionic radii and ionic stiffness, respectively. The parameters used in the present calculations are listed in table 4. Since we consider covalency for the Mo–O bond only, D_{ij}, β_{ij}, and r_{ij}^* are given for this bond. The parameters were set to the values shown in table 5 in order to obtain the best agreement between the observed (Raman and infrared (not discussed here) results) and calculated frequencies.

The atomic displacement vectors for some Raman active modes of $KFe(MoO_4)_2$ are shown in figure 4. In this figure, the numbers are for calculated frequencies in units of cm^{-1}, and the numbers in parentheses are for experimental values also in units of cm^{-1}. The results of the calculations show that the A_{1g} modes at 983 (976) cm^{-1}, 939 (927) cm^{-1} and the E_g mode at 797 (766) cm^{-1} should be assigned to the stretching modes of the MoO_4^{2-} units. Note that the displacement vectors corresponding to the 939 cm^{-1} A_{1g} mode (observed at 927 cm^{-1}) involve very large stretching motion of that Mo–O(1) bond which projects into the interlayer. This mode has an unusually narrow linewidth (∼2.5 cm^{-1}) and its frequency is practically constant under temperature variation, thus indicating a quasi-harmonic behaviour [6]. The large displacement along Mo–O(1) bond is in agreement with polarized Raman measurements

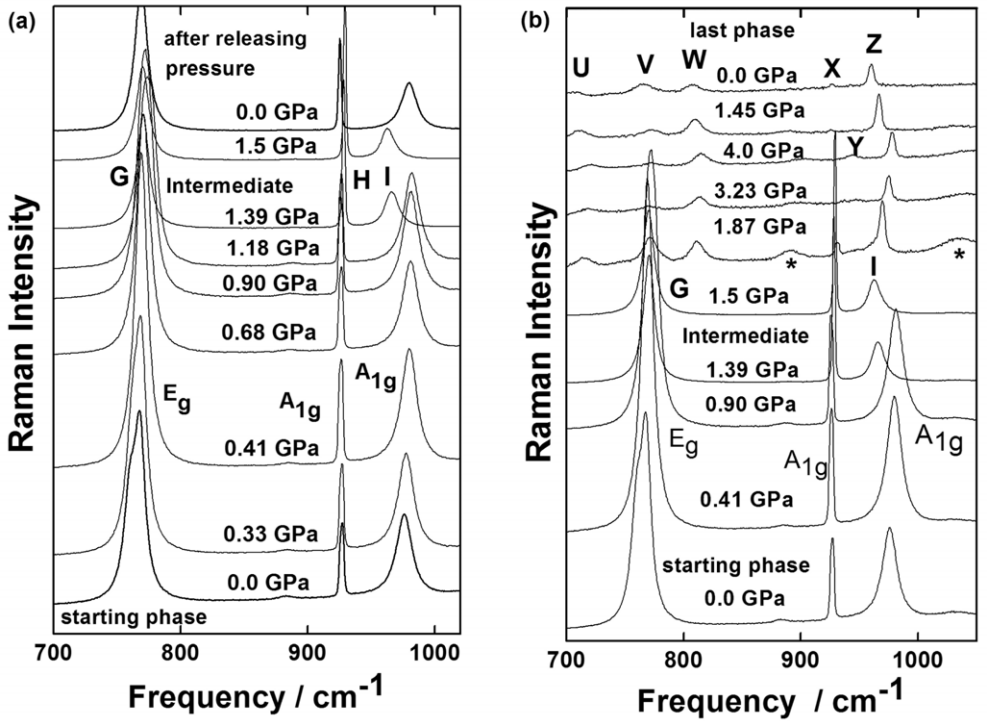

Figure 3. (a) Raman spectra of $KFe(MoO_4)_2$ crystal in the high frequency region recorded at different pressures during compression and decompression experiments performed in the 0–1.5 GPa pressure range. (b) The same as in (a) except that the data are for the 0–4.0 GPa pressure range. The peaks marked with an asterisk relate to the most intense modes of ethanol (888 cm^{-1}) and methanol (1033 cm^{-1}) [20].

Table 5. Potential parameters used for the lattice dynamics calculations of $KFe(MoO_4)_2$.

Ion	z (e)	a (Å)	b (Å)	C (kcal$^{1/2}$ Å^3 mol$^{-1/2}$)
O	−1.05	1.926	0.16	20
K	0.6	1.674	0.09	15
Fe	2.2	0.854	0.08	0
Mo	2.8	0.814	0.09	0
Ion pair	D_{ij} (kcal mol^{-1})	β_{ij} (Å)	r^*_{ij} (Å)	
Mo–O	28.0	2.3	1.92	

which indicate that in (zz) polarization it is much stronger than in (xx) geometry. The remaining stretching modes involve large stretching motions of the other Mo–O(2) bond (figure 4). The same behaviour was also observed for previously studied $KSc(MoO_4)_2$ [6]. According to the calculations the two Raman bands at 495 (368) cm^{-1} and 362 (341) cm^{-1} can be assigned to the bending modes. In the same frequency region a third bending mode should be observed, which did not appear in our spectra. The calculations show also that the 167 (149) cm^{-1} band can be assigned to the A_{1g} translation of the MoO_4^{2-} ions. The E_g modes at 186 (172) cm^{-1} and 116 (60) cm^{-1} involve translational and librational motions of the MoO_4^{2-} ions.

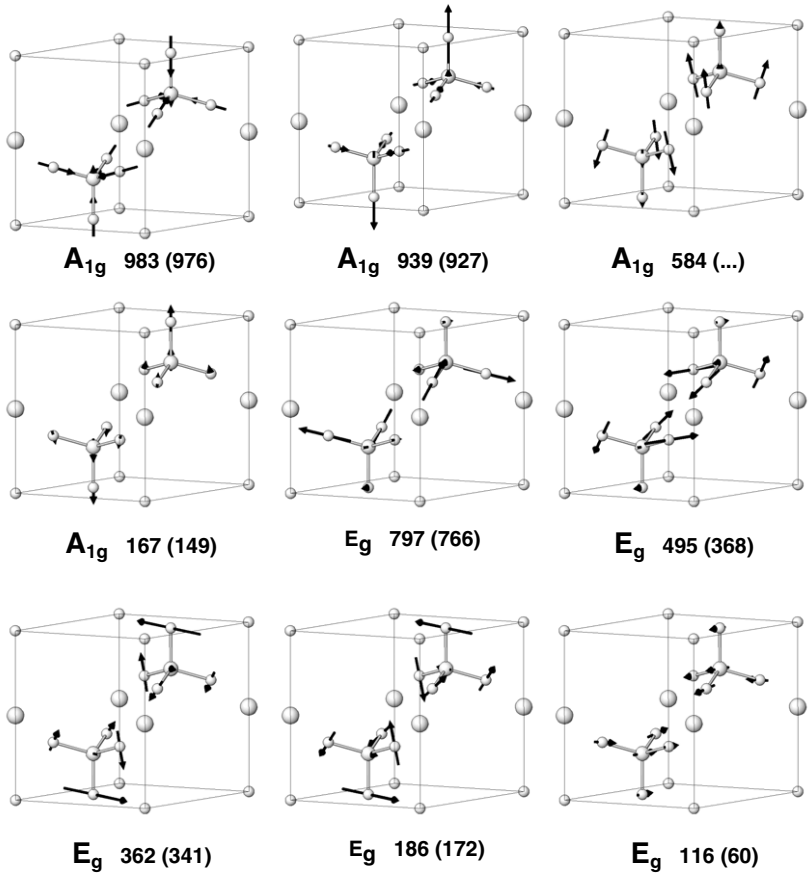

Figure 4. Calculated frequencies in units of cm^{-1} of the Raman active modes for $KFe(MoO_4)_2$ crystals and their related atomic displacements. The experimental frequencies are in parentheses.

3.3. Pressure dependent Raman studies

Once a clear picture of the vibrational properties of the trigonal phase of $KFe(MoO_4)_2$ is obtained we next discuss the effects of hydrostatic pressure on the structural and vibrational properties of this compound. The Raman spectra of $KFe(MoO_4)_2$ crystal measured at several pressures and room temperature are shown in figures 2 and 3. The figures show spectra for the two kinds of experiments performed, the first, for which the releasing pressure value started from 1.5 GPa, and the second, for which this releasing started at 4.0 GPa. At room temperature the crystal symmetry is monoclinic as a result of the lowering of symmetry occurring below $T_1 = 312$ K. One expects, therefore, to observe at room temperature more modes than predicted for the trigonal phase. However, the monoclinic distortion at room temperature is very small and the Raman spectrum looks nearly the same as the spectrum of isomorphic trigonal $KSc(MoO_4)_2$, studied previously by Saraiva *et al* [6]. The only visible influence of the $T_1 = 312$ K phase transition is the presence of a weak splitting of the E_g band observed around 766 cm^{-1} (see the lower trace in figure 3(b)).

The two modes at ∼766 cm^{-1} are not well resolved because, at room temperature, the crystal is very close to the monoclinic–trigonal structure transformation (the onset of this transition being 312 K). On applying pressure, the separation of these E_g modes decreases

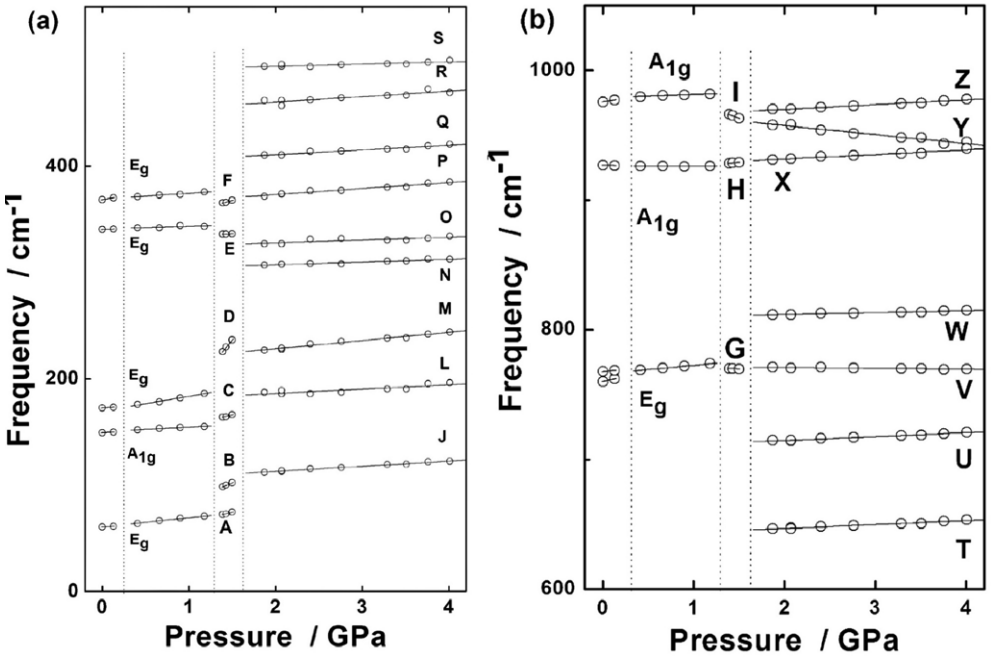

Figure 5. Frequency versus pressure plot in the low frequency (a) and high frequency (b) regions observed during compression. The solid lines are linear fits of the data to $\omega(P) = \omega_0 + \alpha P$. The vertical lines indicate the pressures at which the phase transitions take place.

with pressure and at 0.25 GPa a single peak replaces the two bands. This change could not be taken as continuous because the slopes in the frequency dependence on the pressure are large. As a consequence, the separation would be zero at a pressure value higher than 0.25 GPa, if the change was continuous.

For pressures higher that 1.3 GPa a qualitative change is observed with significant frequency and intensity changes occurring in the Raman spectra. Moreover, new peaks show up in the low frequency region (see figures 2(a) and (b) and 5(b)). These changes indicate that at this pressure a second phase transition takes place. Upon further increase of pressure, remarkable changes in the Raman spectra become evident when the pressure is close to 1.6 GPa. The number of observed modes is nearly doubled and many modes exhibit drastic intensity changes. The narrow peak at 927 cm^{-1} decreases in intensity with pressure and becomes very weak for $P > 3$ GPa. The observed changes indicate the onset of a third pressure induced phase transition at about 1.6 GPa.

The overall changes in the Raman spectra can be appreciated by analysing the frequency (ω) versus pressure (P) plot shown in figure 5. For all peaks the $\omega(P)$ behaviour can be described using a linear function ($\omega(P) = \omega_0 + \alpha P$). The data were fitted to this expression through the least squares method. The results for pressure coefficients of all Raman modes are listed in table 6.

The results shown in figure 5 clearly indicate that the material experiences a first structural phase transition at about 0.25 GPa. Since the most characteristic feature in the 0–0.25 GPa pressure range is a continuous decrease of the ∼766 cm^{-1} E_g mode splitting, the Raman spectra indicate that the monoclinic distortion of the unit cell decreases continuously with increasing pressure. The observation of a single peak at ∼766 cm^{-1} for $P \geqslant 0.25$ GPa in this

Table 6. Pressure intercepts ω_0 and pressure coefficients α for high pressure phases of $KFe(MoO_4)_2$.

$\omega(P) = \omega_0 + \alpha P$									
Intermediate phase Phase II			Intermediate phase Phase III			High pressure phase Phase IV			
Band	ω_0 (cm^{-1})	α (cm^{-1} GPa^{-1})	Band	ω_0 (cm^{-1})	α (cm^{-1} GPa^{-1})	Band	ω_0 (cm^{-1})	α (cm^{-1} GPa^{-1})	Assignment
A_{1g}	978.7	2.6	I	1005.4	−28.3	Z	962.7	3.6	$\nu_1(MoO_4)$
						Y	971.6	−7.0	$\nu_1(MoO_4)$
A_{1g}	925.9	0.2	H	916.3	8.5	X	924.8	3.5	$\nu_3(MoO_4)$
						W	808.5	1.5	
E_g	766.1	6.5	G	774.9	−3.3	V	772.0	−0.6	
						U	708.8	3.0	
						T	640.7	3.0	
						S	489.6	2.2	$\nu_2, \nu_4(MoO_4)$
						R	450.1	5.1	
						Q	402.1	4.4	
E_g	369.1	5.3	F	333.6	22.9	P	361.7	5.7	
E_g	341.2	2.3	E	332.9	2.3	O	322.4	2.7	
						N	301.9	2.6	
E_g	169.4	14.2	D	89.2	98.3	M	213.1	7.7	$T'(MoO_4)$
A_{1g}	150.3	4.1	C	135.6	20.4	L	178.1	4.0	$T'(MoO_4)$
			B	49.9	35.0	J	103.2	4.9	$L(MoO_4)$
A_{1g}	60.5	8.9	A	45.2	19.6				$L(MoO_4)$

pressure range can, therefore, be attributed to the phase transition from the monoclinic phase (phase I in table 6) into the $P\bar{3}m1$ structure (phase II in table 6). This structure corresponds to the phase observed at ambient pressure for temperatures above $T_1 = 312$ K. This result indicates that $\partial T_1/\partial P < 0$.

On further increasing the pressure, the Raman spectra remain qualitatively the same up to 1.3 GPa, except for the upshift observed for all peaks due to compression. The highest $\partial\omega/\partial P$ is observed for the 169.4 cm^{-1} mode in this intermediate pressure range.

The changes observed at ∼1.3 GPa indicate that the $KFe(MoO_4)_2$ crystal exhibits a second phase transition. The most characteristic features of this phase transition are: (i) a significant frequency decrease of the highest frequency Raman mode; (ii) a large intensity change of the 377 cm^{-1} (at 1.19 GPa) mode; (iii) a very large frequency change of the 172 cm^{-1} mode (observed at 186 cm^{-1} at 1.19 GPa) and the appearance of new modes close to 99 cm^{-1}. No splitting of the doubly degenerate modes, including the particular mode close to 766 cm^{-1}, could be observed. These results indicate that the crystal experiences relatively weak structural changes at the phase transition and its symmetry remains trigonal. We believe, therefore, that this phase transition happens to the structure having to $P\bar{3}c1$ symmetry (phase III in table 6). This sequence of phase transition was previously observed in the temperature dependent studies of $RbFe(MoO_4)_2$ [7]. It was shown that at $T_c = 190$ K, the $RbFe(MoO_4)_2$ crystal experiences changes very similar to those observed near 1.3 GPa for $KFe(MoO_4)_2$. Such striking similarity between the Raman spectra observed for the two compounds gives a very strong indication that the mechanism of the pressure induced phase transition in $KFe(MoO_4)_2$ is the same as that of the temperature induced phase transition in $RbFe(MoO_4)_2$. The $P\bar{3}c1$ structure, as mentioned above, is very similar to the $P\bar{3}m1$ structure. It can be obtained from the $P\bar{3}m1$ structure by small rotations of the MoO_4^{2-} tetrahedra along the threefold axis, in opposite directions in the

neighbouring unit cells along the c axis. Factor group analysis for the $P\bar{3}c1$ structure, reported by us and by Klimin *et al* [7, 19], shows that as a result of the $P\bar{3}m1$ to $P\bar{3}c1$ phase transition all E_g modes should split into doublets (see table 4). The A_{1g} modes should also split into doublets ($A_{1g} + A_{2g}$), but since the A_{2g} modes are Raman inactive, we should observe in our experiment only single lines for these modes. Inspection of table 4 shows also that the A_{2g} librational mode and E_u translational mode of the K^+ ions, which are Raman inactive for the $P\bar{3}m1$ phase, should be observed for the $P\bar{3}c1$ phase since they should split into $A_{1g} + A_{2g}$ and $E_u + E_g$ components, respectively.

Our results show that the doubling of the E_g modes is not observed, but a new lattice mode gives rise to a peak at 99 cm^{-1} (peak B in figure 2(b)). Our lattice dynamics calculations suggest that this mode can be attributed to MoO_4^{2-} libration. A K^+ ion translational mode is also expected to make a contribution in the spectra. Although a very weak structure was observed to appear at 58 cm^{-1} in the spectrum taken at 1.5 GPa, its linewidth was too small compared with the currently observed Raman bands and we disregarded this peak. It should be recalled at this point that the lack of this mode can be explained since weakly polarizable K^+ ions should either give rise to very weak Raman bands or no band at all. This agrees with the previous report by Klimin *et al* for $RbFe(MoO_4)_2$ since the $T'(Rb^+)$ translational modes do not manifest in their Raman spectra either. It is noticeable that the highest frequency lattice mode (173 cm^{-1} at ambient pressure), which experienced the largest frequency shift at the phase transition, exhibits also an unusually high $\partial\omega/\partial P$ value (98.3 cm^{-1} GPa^{-1}; see table 6), an order of magnitude larger than the values observed for the phases I and II. Moreover, the highest frequency Raman mode exhibits an unusually large negative $\partial\omega/\partial P$ value (-28.3 cm^{-1} GPa^{-1}). The origin of this peculiar behaviour is not completely understood but it indicates that pressure induces large changes in the Mo–O–Fe distances and angles due to significant rotations of FeO_6 octahedra and MoO_4^{2-} tetrahedra.

The third phase transition occurs at about 1.6 GPa. The analysis of the Raman spectra indicates that this transition has first-order character and the material undergoes drastic structural changes. First of all it should be said that this transition leads to significant distortion of the MoO_4^{2-} tetrahedra. This is clearly seen since the stretching and bending mode spread over broader regions (646–970 and 307–495 cm^{-1}) than in the phases observed below 1.6 GPa, thus meaning a much larger distribution of Mo–O bond lengths. Since the number of modes increases when the phase transition takes place, the high pressure phase (denoted as phase IV in table 6) has symmetry lower than trigonal. It is clear from figure 5(b) that stretching modes split into seven components. Since there are four stretching modes for a MoO_4^{2-} unit, the observation of seven components indicates that this new phase has two non-equivalent MoO_4^{2-} units occupying low symmetry sites. As a result of this transition, large changes are also observed for the narrow stretching mode observed near 927 cm^{-1}. The intensity of this mode decreases and bandwidth increases rapidly with increasing pressure. Since this mode corresponds to vibration of that oxygen atom which projects into the layer and interacts only with K^+ ions, the observed changes show that K–O bonds are also strongly affected by this transition. The pressure dependence of the vibrational modes is not only much weaker than that observed for the phase stable in the 1.3–1.6 GPa range, but also weaker than that observed for phases I and II. The Raman study suggests, therefore, that the structure of this phase is more compact, but tetrahedral coordination of molybdenum atoms is preserved.

In order to get new insight into the mechanism of phase transitions in $KFe(MoO_4)_2$, we have also performed Raman studies of $KFe(MoO_4)_2$ crystal during the decompression. This study shows that upon releasing the pressure from 1.5 GPa, i.e. from the pressure at which the intermediate trigonal phase III is stable, the starting phase I was not recovered (see figures 2(a) and 3(a)). In figure 6, we show the spectra taken at 0.0 GPa for the starting phase and after

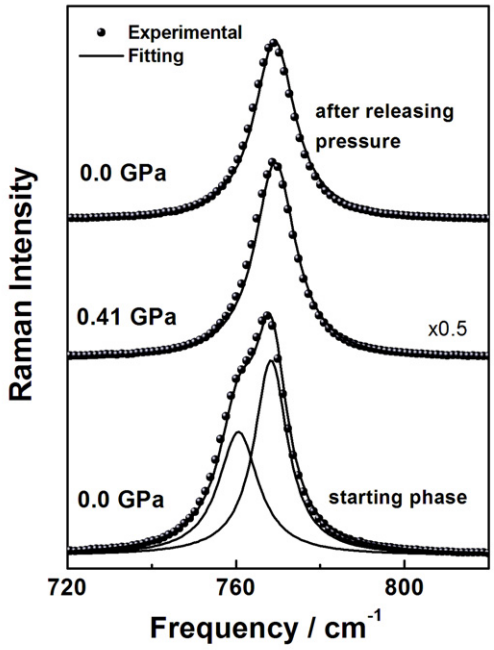

Figure 6. Raman spectra of $KFe(MoO_4)_2$ crystals recorded at 0.0 GPa before (lower trace) and after compression (upper trace). The maximum pressure attained in this run was 1.5 GPa. The intermediate trace stands for the spectrum recorded at 0.41 GPa during the compression run where the $P\bar{3}c1$ phase is stable.

releasing the pressure, as well as the phase at 1.5 GPa. We can note that the feature associated with the monoclinic phase (splitting of the E_g mode) is not observed in the spectra obtained at 0.0 GPa after releasing the pressure. This indicates that the transition from monoclinic to $P\bar{3}m1$ (from $P\bar{3}m1$ to $P\bar{3}c1$) observed at 0.25 GPa (1.35 GPa) is not (is) reversible. This result shows that the energy difference between the two polymorphs is very small and probably some defects induced by pressure or some level of residual strain are enough to stabilize the trigonal phase. When the sample is transformed to the low symmetry, high pressure phase IV above 1.3 GPa, however, the starting phase is not recovered upon releasing pressure down to the ambient conditions (see figures 2(b) and 3(b)). It is obvious from this experiment that the phase transition into phase IV is irreversible.

3.4. X-ray study of the high pressure phase

X-ray diffraction patterns of the $KFe(MoO_4)_2$ sample subjected to a 4.0 GPa pressure and recovered from the diamond anvil cell are presented in figure 7. As one can note, the number of diffraction lines increased significantly but the main lines of the pristine sample remained. At a glance, this result suggests that the recovered sample could be a mixture of the high pressure and the pristine phase. However, this hypothesis can be ruled out for two reasons: first, the $2\theta = 37.96°$ diffraction line of the pristine $KFe(MoO_4)_2$ is not observed in the diffractogram of the recovered sample (see figure 7). Second, our Raman experiment shows that $KFe(MoO_4)_2$ transforms completely and irreversibly to a high pressure phase just as the pressure value

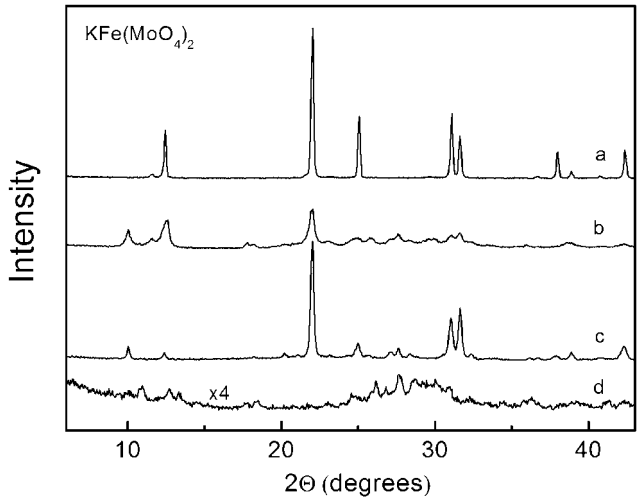

Figure 7. Powder x-ray diffraction patterns of pristine $KFe(MoO_4)_2$ at ambient pressure (a), the sample processed at 4 GPa pressure (b), the sample processed at 4 GPa pressure and then heated up to 653 K (c), and the sample processed simultaneously at 4 GPa and 673 K (d).

1.6 GPa is attained. We conclude, therefore, that all diffraction peaks for the recovered sample come from the high pressure phase. Our attempt to index the recorded diffractograms were not successful in hexagonal/trigonal or orthorhombic systems. The monoclinic unit cell can be found, but with so many solutions that it is not possible to choose a unique one. It is also worth noting that the diffraction lines of the high pressure phase are much broader than those observed for the pristine sample. This points to some disorder induced in the high pressure structure. Another possible reason for the peak broadening is the reduction of the crystallite size or residual strain. Only a systematic study of the angular dependence of the peak broadening could help to identify its origin. However, our present data set is not suitable for such study, and we hope to further clarify this issue in a forthcoming publication. Anyway, the presence of the halo in the x-ray diffractogram indicates a partial amorphization of the sample and, accordingly, the broadening of the other peaks may be associated with disorder rather than crystallite size effects.

In order to get new information about the stability of the high pressure phase two experiments were performed. In the first experiment, the sample processed at high pressure was subjected to heat treatment at 653 K. In the second experiment, the same sample was processed simultaneously at a temperature of 673 K and a pressure of 4 GPa (see the experimental section). The observation of the sample obtained in the first experiment revealed that it is composed of two phases, brown and green–yellow. The measured x-ray diffractogram shows that the majority of lines agree well with the x-ray pattern of the original high pressure phase, but the lines become narrower (see figure 7). This result indicates that heating the sample to 653 K leads to a decrease of disorder due, most probably, to relaxation of defects. However, the appearance of the brown phase indicates also that part of the sample either decomposes or transforms into another phase. The sample obtained in the second experiment is brown and does not contain the green–yellow phase. The x-ray diffractogram shows that the most characteristic lines of the high pressure phase disappear (see figure 7). This result shows that the green–yellow high pressure phase is unstable at higher temperatures. The open question remains, however, of what kinds of changes occur in this material. The high pressure phase could transform into

another polymorph or could decompose. The attempts to identify the decomposition products, such as iron oxides, MoO_3, and several iron molybdates, have however not yet been successful.

4. Conclusions

High temperature x-ray and room temperature pressure dependent Raman studies of layered $KFe(MoO_4)_2$ were performed here. The results show that the crystal structure of this material at ambient pressure and above 312 K is $P\bar{3}m1$. Below 312 K the crystal structure is monoclinic. Upon increasing the pressure the monoclinic phase transforms to the $P\bar{3}m1$ structure at 0.25 GPa. Our studies also show that this material exhibits another reversible phase transition when the pressure is close to 1.3 GPa to, most probably, the $P\bar{3}c1$ phase. In addition, an irreversible phase transition occurs at 1.6 GPa to a low symmetry phase. Although the structure of this high pressure phase could not be established, the x-ray diffraction studies performed for the crystal recovered from the highest pressure phase upon releasing the pressure revealed that this phase is monoclinic or triclinic. This finding agrees with our previous studies of $KSc(MoO_4)_2$ where a pressure induced irreversible phase transition into a low symmetry phase was found. This phase is characterized by two crystallographically non-equivalent and strongly distorted MoO_4^{2-} tetrahedra. This result indicates that the highest pressure phases of $KFe(MoO_4)_2$ and $KSc(MoO_4)_2$ have similar structures. In addition we show that the driving mechanism of the phase transitions here is the same as in the $KSc(MoO_4)_2$ molybdate. These transitions are associated with rotations of the MoO_4^{2-} tetrahedra that lead to an increase in electrostatic repulsion between oxygen atoms and consequently to instability of the structures. However, the important difference between these crystals is that $KFe(MoO_4)_2$ exhibits the presence of an intermediate trigonal phase, most probably of $P\bar{3}c1$ structure. Within the numerous works on layered trigonal molybdates and tungstates, the $P\bar{3}m1$ to $P\bar{3}c1$ phase transition was reported previously only for $RbFe(MoO_4)_2$ (in a temperature dependent experiment). It is possible to conclude, therefore, that the distinct behaviours of the scandium and iron analogues may be due to the difference in electronic and magnetic properties of Fe^{3+} and Sc^{3+}.

Acknowledgments

AGSF acknowledges financial support from the Brazilian agency FUNCAP (Grant PPP-985/03) and a research fellowship from CNPq (Grant 307417/2004-2).

References

[1] Otko A I, Nesterenko N M and Povstyanyi L V 1978 *Phys. Status Solidi* a **46** 577
[2] Nesterenko N M, Fomin V I and Zvyagin A I 1979 *Izv. Akad. Nauk. SSSR* **43** 1675
[3] Zapart W 1990 *Phys. Status Solidi* a **118** 447
[4] Zapart M B and Zapart W 1993 *Phase. Transit.* **43** 173
[5] Maczka M, Kojima S and Hanuza J 1999 *J. Phys. Soc. Japan* **68** 1948
[6] Saraiva G D, Maczka M, Freire P T C, Mendes Filho J, Melo F E A, Hanuza J, Morioka Y and Souza Filho A G 2003 *Phys. Rev.* B **67** 224108
[7] Klimin S A, Popova M N, Mavrin B N, Van Loosdrecht P H M, Svistov L E, Smirnov A I, Prozorova L A, Krug van Nidda H A, Seidov Z and Loidl A 2003 *Phys. Rev.* B **68** 174408
[8] Svistov L E, Smirnov A I, Prozorova L A, Petrenko O A, Shapiro A Ya and Demianets L A 2004 *Pis. Zh. Eksp. Teor. Fiz.* **80** 231 (in Russian)
[9] Jorge G A, Capan C, Ronning F, Jaime M, Kenzelmann M, Gasparovic G, Broholm C, Shapiro A Ya and Demianets L A 2004 *Physica* B **354** 297

[10] Klevtsova R F and Klevtsov P V 1970 *Kristallografiya* **15** 953 (in Russian)
[11] Efremov V A, Trunov V K and Velokodnyi Yu A 1973 *Sov. Phys.—Crystallogr.* **17** 1005
[12] Tomaszewski P E, Pietraszko A, Maczka M and Hanuza J 2002 *Acta Crystallogr.* E **58** i119
[13] Krainyuk G G, Otko A I and Nosenko A E 1983 *Izv. SSSR Ser. Fiz.* **47** 758 (in Russian)
[14] Oxford Diffraction 2002 *CrysAlis RED version 1.170.14* (Oxford, UK: Oxford Diffraction Ltd)
[15] Sheldrick G M 1997 *SHELXL97, Program for Solution of the Crystal Structures* University of Goettingen
[16] Sherman W F and Stadtmuller A A 1987 *Experimental Techniques in High-Pressure Research* (London: Wiley)
[17] Khvostantsev L G 1984 *High Temp.—High Pressures* **16** 165
[18] Nozaki R, Kondo J N, Hirose C, Domen K, Wada A and Morioka Y 2001 *J. Phys. Chem.* B **105** 7950
[19] Maczka M, Hanuza J, Kojima S and van der Maas J H 2001 *J. Solid State Chem.* **158** 334
[20] Lemos V and Camargo F 1990 *J. Raman Spectrosc.* **21** 123